Modeling and Control of Contouring Errors for Five-Axis Machine Tools—Part I: Modeling

Burak Sencer
Ph.D. Candidate

Yusuf Altintas
Professor,
ASME Fellow

Elizabeth Croft
Professor

Manufacturing Automation Laboratory,
University of British Columbia,
Vancouver, BC, V6T 1Z4, Canada

Aerospace, die, and mold industries utilize parts with sculptured surfaces, which are machined on five-axis computer numerical controlled machine tools. Accurate path tracking for contouring is not always possible along the desired space curves due to the loss of joint coordination during the five-axis motion. This two-part paper presents modeling and robust control of contouring errors for five-axis machines. In Part I, two types of contouring errors are defined by considering the normal deviation of tool tip from the reference path, and by the normal deviation of the tool axis orientation from the reference orientation trajectory defined in the spherical coordinates. Overall contouring errors are modeled during five-axis motion that has simultaneous translation and rotary motions. The coupled kinematic configuration and the rigid body dynamics of all five drives are considered. The contouring error model is experimentally validated on a five-axis machine tool. The error model developed in this paper is then used for simultaneous, real-time robust control of all five drives in Part II. [DOI: 10.1115/1.3123335]

1 Introduction

Five-axis computer numerical controlled (CNC) machine tools are widely used in machining parts with complex sculptured surfaces such as dies, molds, and aerospace parts. The ultimate goal of for these industrial machining applications is to attain high dimensional accuracy in five-axis machining at fast cutting and feed speeds. However, the dimensional accuracy of the part is affected by the relative structural and thermal deformations of the tool and workpiece, volumetric accuracy of the machine tool [1], and contouring errors induced by the feed drive control system. Each drive on the machine tool is subject to unavoidable tracking errors between the commanded and actual positions due to the servo controller dynamics. These tracking errors are kinematically transformed to the tool tip, resulting in contouring errors between the commanded tool-path and actual path delivered by the CNC unit.

The dedicated control law of each drive tries to minimize the tracking error $(e_x, e_y, e_z, \ldots)$ independent of other drives. As a consequence of the non-Cartesian kinematics of the five-axis machine tool, small tracking errors on rotary axes may result in larger deviations of the tool tip from the reference tool-path relative to the workpiece. In addition, when one axis is subject to a disturbance, other axes will perform as if the disturbed axis is functioning normally. This results in a loss of coordination and degradation of the overall contouring accuracy.

The *contour error* (ε), which is defined as the orthogonal deviation from the desired tool-path [2], is the actual measure of the part accuracy. Figure 1 shows the relationship between contour error and the axis tracking errors for simple linear and curved tool-paths. When following a linear tool-path (see Fig. 1(*a*)), the contour error (ε) can be expressed as a simple analytical function of the axis tracking errors (e_x, e_y) as

$$\left.\begin{aligned} \varepsilon &= -C_x e_x + C_y e_y \\ C_x &= \sin(\theta) \\ C_y &= \cos(\theta) \end{aligned}\right\} \quad (1)$$

On the other hand, while machining curved tool-path such as *B*-splines or Nurbs, accurate computation of the contour errors becomes more challenging (Fig. 1(*b*)). Koren and Lo [3] used Eq. (1) in estimating the contour errors in two-axis machining along simple linear tool-paths. They proposed the first cross coupling control (CCC) algorithm to reduce the normal deviation of the tool tip from the path. Later, Koren and Lo [4] extended the contour error estimation to design a CCC algorithm for circular tool-paths. Erkorkmaz and Altintas [5] estimated the contour error along arbitrary tool-paths by computing the Euclidian distance from the desired tool-path to the actual tool position in the vicinity of n number of interpolated points, and identified the reference point with the minimum deviation from the actual tool tip. The contour error vector was then defined to be normal to the vector between the identified and the consecutive reference path points. As a result, the shortest vector normal to the desired contour is obtained, but the computationally intensive nature of the iterative solution proposed was undesirable for real-time control. Chiu and Tomizuka [6] developed an analytical contour error estimation procedure for two-axis machining of C^2 continuous curved tool-paths. They reflected the tracking errors of the Cartesian axes on the tangent and normal directions of the tool-path, and considered the error component in the normal direction as the approximation of actual contour error. Later, Yeh and Hsu [7] defined the gains $C_x(t), C_y(t)$ in Eq. (1) to vary as a function of the time. Thus, they were able to estimate contour errors also for splines and curved paths. The contour error approximation becomes inaccurate if the error in tangent direction is high. This occurs particularly during high speed machining of paths with sharp curvature changes. Peng and Chen [8] attacked this problem and modified the previous approximations with addition of an extra term so that the overcutting of the path is avoided in two-axis Cartesian motions. Apart from Cartesian contouring systems, Katz et al. [9] addressed the contouring problem on a nonorthogonal reconfigurable three-axis machine tool. They modeled the kinematics of the machine tool and designed time varying gains for Eq. (1) in order estimate the contour errors. Lin and Hu [10] used the kinematics of a five-axis machine tool and estimated contour errors of the tool tip only as

Contributed by the Manufacturing Engineering Division of ASME for publication in the JOURNAL OF MANUFACTURING SCIENCE AND ENGINEERING. Manuscript received July 14, 2008; final manuscript received February 27, 2009; published online May 1, 2009. Review conducted by Eric R. Marsh.

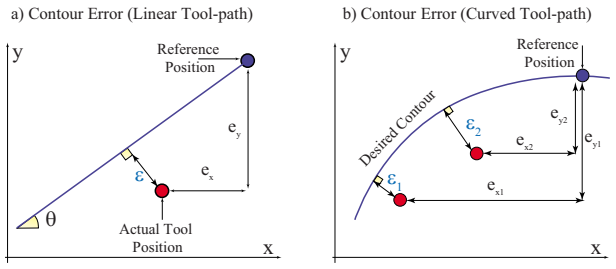

Fig. 1 Definition of contour errors in two-axis Cartesian machining

the difference between the reference and the actual circle radii, during simple circular interpolation. Later, Lo [11] designed coupled proportional-integral-derivative (PID) controllers and showed that minimizing the tracking errors of the tool tip in the workpiece coordinates results in better contouring performance.

Past literature has been mainly addressed the contouring control problem for three-axis Cartesian machining applications, where the contour error is simply defined as the norm of the translational deviation of the tool tip from the reference tool-path. However, the tool translates and rotates to follow the reference orientation in five-axis machining [12,13] (Fig. 2(*a*)), producing both the "tool tip contour error" and the "tool orientation contour error," as illustrated in Fig. 2(*b*). Similar to two- or three-axis Cartesian machining applications, tool tip contour error is very important for avoiding both overcutting and undercutting during general point milling operations. On the other hand, the tool orientation contour error is defined as the normal angular deviation of the tool axis from desired orientation trajectory. As shown in Fig. 2(*b*), orientation contour error becomes detrimental to part tolerances, especially in flank milling operations where the cutting is performed mainly along the tool axis. Consequently, when using flat or toroidal end mils, the combination of the tool tip and tool orientation errors causes gouging of the workpiece. In order to attain desired part tolerances, both the tool tip and the tool axis orientation contour errors need to be controlled.

This two-part paper series presents the modeling and control of contouring errors in five-axis machining. Part I presents the modeling of five-axis machine kinematics, dynamics, and the prediction of the contour errors. Section 2 describes the kinematic modeling of the five-axis machine tool, which is then used in the formulation of the general tracking error dynamics of the tool during five-axis motion. The prediction model for tool tip and orientation contouring errors is presented in Sec. 3. The predicted contour errors are compared experimentally against the measured errors in Sec. 4, and the paper is concluded in Sec. 5. The contour error model is later used in the design of a sliding mode contour error controller that is presented in Part II of the series.

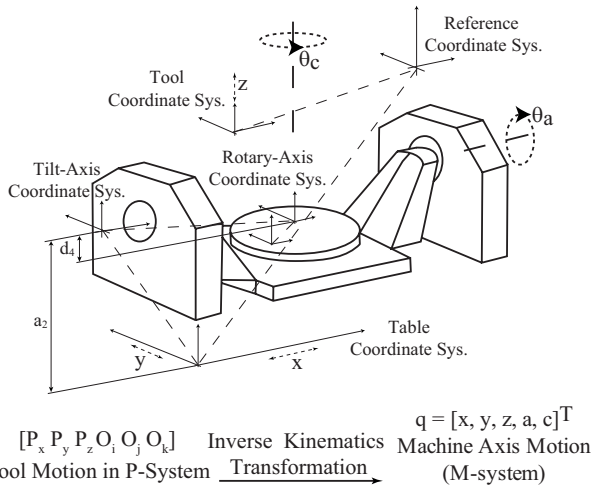

Fig. 3 Tilting rotation table (TRT) five-axis machine tool

2 Kinematic Model of Five-Axis Machine

The motion of the tool during five-axis contouring operation depends on the movement of the physical drives of the machine tool. A widely used, tilting-rotary-table type kinematic configuration [14] is taken as an example here, as illustrated in Fig. 3. The five-axis machine has three translational motions, x, y, and z, combined with the rotations θ_a and θ_c of the a and c rotary drives, respectively. The tool positions are expressed in the workpiece coordinate system (P-system) by the position vector of the tool tip $\mathbf{P}(t)=[P_x(t),P_y(t),P_z(t)]^T$, and by the unit vector defining the tool axis orientation $\mathbf{O}(t)=[O_i(t),O_j(t),O_k(t)]^T, |\mathbf{O}|=1$ (see Fig. 2(*a*)).

The reference tool-path variables (P_x,P_y, P_z, O_i, O_j, and, O_k) in the P-system are transformed into position commands of the physical drives of the machine tool

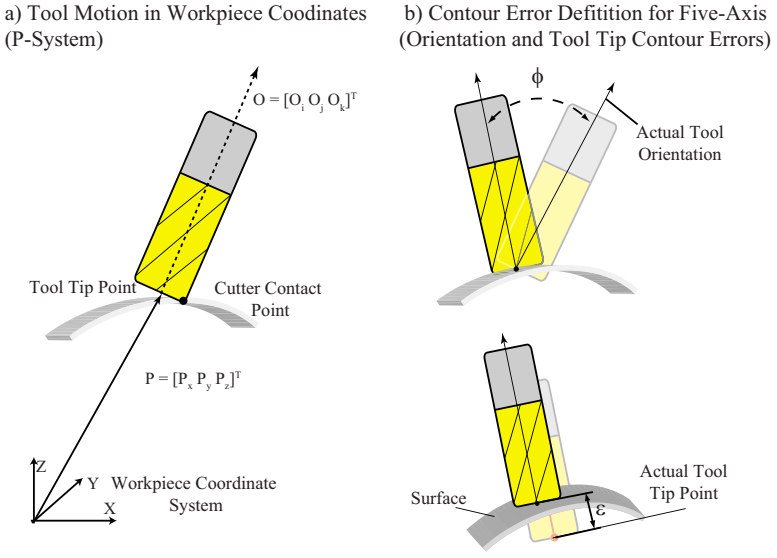

Fig. 2 Tool motion in workpiece coordinates (*P*-system)

$$\mathbf{q}(t) = [x(t), y(t), z(t), \theta_a(t), \theta_c(t)]^T \tag{2}$$

where x, y, z, θ_a, and θ_c are the axis coordinates in the machine tool coordinate system (M-system).

The transformation from the P-system to the M-system is carried out using an inverse kinematics transformation in two steps [15]. The angular motions of the rotary axes are obtained from

$$\begin{aligned} \theta_a &= -\sin^{-1}(O_k) \quad ,(-\pi < a \le \pi) \\ \theta_c &= \tan^{-1}(O_i, O_j) \quad ,(O_i = O_j \neq 0) \end{aligned} \tag{3}$$

which are kinematically transformed to define the tool axis direction as

$$\underbrace{\begin{bmatrix} O_i \\ O_j \\ O_k \end{bmatrix}}_{\mathbf{O}} = \begin{bmatrix} \cos\theta_a \sin\theta_c \\ \cos\theta_a \cos\theta_c \\ -\sin\theta_a \end{bmatrix} \tag{4}$$

The rotary axis velocities ($\dot{\theta}_a(t)$ and $\dot{\theta}_c(t)$) are related to the angular velocity vector ($\boldsymbol{\omega}(t)=[\dot{O}_i(t), \dot{O}_j(t), \dot{O}_k(t)]^T$) of the tool by the orientation Jacobian $\mathbf{J}_O \in \Re^{3\times 2}$ of the machine

$$\underbrace{\begin{bmatrix} \dot{O}_x \\ \dot{O}_j \\ \dot{O}_k \end{bmatrix}}_{\boldsymbol{\omega}} = \underbrace{\begin{bmatrix} -\sin\theta_a \sin\theta_c & \cos\theta_c \cos\theta_c \\ -\sin\theta_c \cos\theta_c & -\cos\theta_c \sin\theta_c \\ -\cos\theta_c & 0 \end{bmatrix}}_{\mathbf{J}_O} \begin{bmatrix} \dot{\theta}_c \\ \dot{\theta}_c \end{bmatrix} \tag{5}$$

The Cartesian axes positions $[x(t)y(t)z(t)]^T$ are evaluated by applying Devanit–Hartenberg method [16] on the machine shown in Fig. 3.

$$\begin{bmatrix} x(t) \\ y(t) \\ z(t) \end{bmatrix} = \begin{bmatrix} -\cos(\theta_c(t)) & \sin(\theta_c(t)) & 0 \\ -\cos(\theta_a(t))\sin(\theta_c(t)) & -\cos(\theta_a(t))\cos(\theta_c(t)) & \sin(\theta_a(t)) \\ \sin(\theta_a(t))\sin(\theta_c(t)) & \sin(\theta_a(t))\cos(\theta_c(t)) & \cos(\theta_a(t)) \end{bmatrix} \begin{bmatrix} P_x \\ P_y \\ P_z \end{bmatrix} + \begin{bmatrix} 0 & 0 \\ \sin(\theta_a(t)) & 0 \\ \cos(\theta_a(t)) & -1 \end{bmatrix} \begin{bmatrix} d_4 \\ a_2 \end{bmatrix} \tag{6}$$

where d_4 and a_2 are linear offsets between the rotary drive coordinate frames. The coordinates of the tool tip position in the P-system can be evaluated from Eq. (2) as a function of the axis positions as

$$\underbrace{\begin{bmatrix} P_x(t) \\ P_y(t) \\ P_z(t) \end{bmatrix}}_{\mathbf{P}} = \begin{bmatrix} -\cos(\theta_c(t)) & -\sin(\theta_c(t))\cos(\theta_a(t)) & \sin(\theta_a(t))\sin(\theta_c(t)) \\ \sin(\theta_c(t)) & -\cos(\theta_c(t))\cos(\theta_a(t)) & \sin(\theta_a(t))\cos(\theta_c(t)) \\ 0 & \sin(\theta_a(t)) & \cos(\theta_a(t)) \end{bmatrix} \begin{bmatrix} x(t) \\ y(t) \\ z(t) \end{bmatrix} + \begin{bmatrix} 0 & -\sin(\theta_c(t))\sin(\theta_a(t)) \\ 0 & -\cos(\theta_c(t))\sin(\theta_a(t)) \\ -1 & -\cos(\theta_a(t)) \end{bmatrix} \begin{bmatrix} d_4 \\ a_2 \end{bmatrix} \tag{7}$$

The direct kinematic transformation (Eq. (7)) shows that translational (x,y,z) and rotational (θ_a, θ_c) drive positions in the M-system govern the tool tip location ($P=[P_x P_y P_z]^T$) on the workpiece surface. Consequently, the tracking error on any drive is reflected on the tool tip; hence, this error will contribute to the contouring error along the path. A "tool pose variable," which will be used later for the controller design, is defined as

$$\mathbf{x}(t) = \left[\underbrace{P_x(t) P_y(t) P_z(t)}_{\mathbf{P}} \vdots\ \theta_a(t)\, \theta_c(t)\right]^T \tag{8}$$

which contains the tool tip location in the P-system and the two rotary drive positions. The partial derivatives of the tool tip coordinates with respect to the axis positions are obtained by differentiating Eq. (7) as follows:

$$J_{ij} = \frac{\partial P_i}{\partial q_j} i \in (x,y,z), \quad q_j \in (x,y,z,\theta_a,\theta_c) \tag{9}$$

and by adding two unity elements on the diagonal for the rotational drive positions, the following square Jacobian matrix ($\mathbf{J}(t) \in \Re^{5\times 5}$) is formed:

$$\mathbf{J}(t) = \begin{bmatrix} J_{11} & J_{12} & J_{13} & J_{14} & J_{15} \\ J_{21} & J_{22} & J_{23} & J_{24} & J_{25} \\ J_{31} & J_{32} & J_{33} & J_{34} & J_{35} \\ 0 & 0 & 0 & 1 & 0 \\ 0 & 0 & 0 & 0 & 1 \end{bmatrix} \tag{10}$$

The Jacobian matrix relates the drive velocities ($\dot{\mathbf{q}}(t)$) and accelerations ($\ddot{\mathbf{q}}(t)$) to the tool pose kinematics ($\dot{\mathbf{x}}(t)$ and $\ddot{\mathbf{x}}(t)$) as

$$\underbrace{\begin{bmatrix} \dot{P}_x \\ \dot{P}_y \\ \dot{P}_z \\ \dot{\theta}_a \\ \dot{\theta}_c \end{bmatrix}}_{\dot{\mathbf{x}}} = \mathbf{J}(t) \underbrace{\begin{bmatrix} \dot{x} \\ \dot{y} \\ \dot{z} \\ \dot{\theta}_a \\ \dot{\theta}_c \end{bmatrix}}_{\dot{\mathbf{q}}}, \quad \underbrace{\begin{bmatrix} \ddot{P}_x \\ \ddot{P}_y \\ \ddot{P}_z \\ \ddot{\theta}_a \\ \ddot{\theta}_c \end{bmatrix}}_{\ddot{\mathbf{x}}} = \mathbf{J}(\mathbf{q}) \underbrace{\begin{bmatrix} \ddot{x} \\ \ddot{y} \\ \ddot{z} \\ \ddot{\theta}_a \\ \ddot{\theta}_c \end{bmatrix}}_{\ddot{\mathbf{q}}} + \dot{\mathbf{J}}(\mathbf{q}, \dot{\mathbf{q}}) \underbrace{\begin{bmatrix} \dot{x} \\ \dot{y} \\ \dot{z} \\ \dot{\theta}_a \\ \dot{\theta}_c \end{bmatrix}}_{\dot{\mathbf{q}}} \tag{11}$$

3 Real-Time Prediction of Contouring Errors

Contour errors left on the finished surface vary as a nonlinear function of the tracking errors of the tool, while the tool moves along the reference tool-path. Tracking errors of the tool, on the other hand, are governed by the machine kinematics and the errors of the axis servo drives.

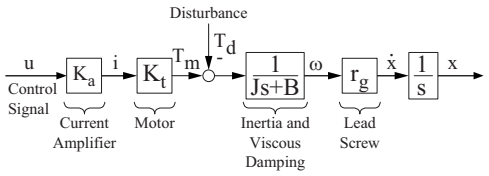

Fig. 4 Axis dynamics

3.1 Tracking Error Dynamics on the Workpiece. The simplified linear dynamics of a typical feed drive system is presented in Fig. 4. The corresponding rigid body model can then be expressed as

$$\underbrace{\begin{bmatrix} m_x & 0 & 0 & 0 & 0 \\ 0 & m_y & 0 & 0 & 0 \\ 0 & 0 & m_z & 0 & 0 \\ 0 & 0 & 0 & m_a & 0 \\ 0 & 0 & 0 & 0 & m_c \end{bmatrix}}_{\mathbf{M}} \underbrace{\begin{bmatrix} \ddot{x} \\ \ddot{y} \\ \ddot{z} \\ \ddot{\theta}_a \\ \ddot{\theta}_c \end{bmatrix}}_{\ddot{\mathbf{q}}} + \underbrace{\begin{bmatrix} c_x & 0 & 0 & 0 & 0 \\ 0 & c_y & 0 & 0 & 0 \\ 0 & 0 & c_z & 0 & 0 \\ 0 & 0 & 0 & c_a & 0 \\ 0 & 0 & 0 & 0 & c_c \end{bmatrix}}_{\mathbf{C}} \underbrace{\begin{bmatrix} \dot{x} \\ \dot{y} \\ \dot{z} \\ \dot{\theta}_a \\ \dot{\theta}_c \end{bmatrix}}_{\dot{\mathbf{q}}} = \underbrace{\begin{bmatrix} u_x \\ u_y \\ u_z \\ u_a \\ u_c \end{bmatrix}}_{\mathbf{u}} - \underbrace{\begin{bmatrix} d_x \\ d_y \\ d_z \\ d_a \\ d_c \end{bmatrix}}_{\mathbf{d}} \tag{12}$$

where $m_i = J_i / K_{ai} K_{ti} r_{gi}$ is the equivalent inertia, $c_i = B_i / K_{ai} K_{ti} r_{gi}$ is viscous damping, $u_i(t)$ is control voltage produced by the digital control law of the drive, $d_i(t)$ is equivalent disturbance, and the suffix $i = x, y, z, a, c$ denotes x, y, z, a, c drives, respectively. K_a and K_t are the amplifier and motor torque constants, and r_g is the gear reduction ratio of the drives. The drive accelerations ($\ddot{\mathbf{q}}$) can be represented in compact form by

$$\ddot{\mathbf{q}}(t) = \mathbf{M}^{-1}[\mathbf{u}(t) - \mathbf{d}(t) - \mathbf{C}\dot{\mathbf{q}}(t)] \tag{13}$$

By substituting the kinematics relationships from Eq. (11) into Eq. (13), the drive dynamics can be mapped to the tool pose as

$$\ddot{\mathbf{x}}(t) = \dot{\mathbf{J}}(t)\dot{\mathbf{q}}(t) + \mathbf{J}(t)\mathbf{M}^{-1}[\mathbf{u}(t) - \mathbf{d}(t) - \mathbf{C}\dot{\mathbf{q}}(t)] \tag{14}$$

The actual position, velocity, and acceleration of the pose can be written as a sum of the reference commands and corresponding tracking errors

$$\mathbf{x}_{\text{ref}}(t) = [P_{x,\text{ref}}, P_{y,\text{ref}}, P_{z,\text{ref}}, a_{\text{ref}}, c_{\text{ref}}]^T, \quad \mathbf{e}(t) = [e_{Px}, e_{Py}, e_{Pz}, e_a, e_c]^T$$
$$\rightarrow \mathbf{e} = \mathbf{x}_{\text{ref}} - \mathbf{x} \tag{15}$$

Substituting Eq. (16) into Eq. (14), the tracking error dynamics of the tool is expressed by

$$\ddot{\mathbf{e}}(t) = \ddot{\mathbf{x}}_{\text{ref}}(t) - \dot{\mathbf{J}}(t)\dot{\mathbf{q}}(t) - \mathbf{J}(t)\mathbf{M}^{-1}[\mathbf{u}(t) - \mathbf{d}(t) - \mathbf{C}\dot{\mathbf{q}}(t)] \tag{16}$$

Note that in Eq. (16), the vector $\ddot{\mathbf{x}}_{\text{ref}}(t)$ is trajectory dependent where $\mathbf{J}(t)$ and $\dot{\mathbf{J}}(t)$ introduce time varying nonlinear coupling since they depend on the drive position as well as on velocities.

3.2 Tool Tip Contour Error Estimation. The reference trajectory of the tool tip ($\mathbf{P}_{\text{ref}} = [P_{x,\text{ref}}, P_{y,\text{ref}}, P_{z,\text{ref}}]^T$), the corresponding tracking errors ($\mathbf{e}_P = [e_{Px}, e_{Py}, e_{Pz}]^T$), as well as the contour error vector ($\boldsymbol{\varepsilon}$) are illustrated in Fig. 5(a). The mutually orthogonal unit tangent, $\mathbf{t}(t)$, and normal, $\mathbf{n}(t)$, vectors along the path are computed using the reference velocity and acceleration of the tool tip;

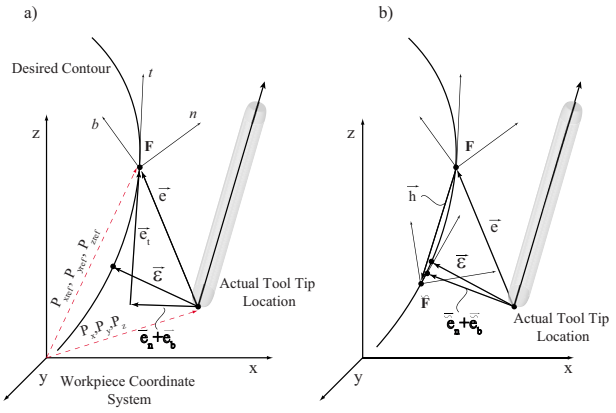

Fig. 5 Tool tip contour error estimation

$$\mathbf{t} = \left[\frac{\dot{P}_{x,\text{ref}}}{\|\dot{\mathbf{P}}_{\text{ref}}\|}, \frac{\dot{P}_{y,\text{ref}}}{\|\dot{\mathbf{P}}_{\text{ref}}\|}, \frac{\dot{P}_{z,\text{ref}}}{\|\dot{\mathbf{P}}_{\text{ref}}\|} \right]^T, \quad \mathbf{n} = \left[\frac{\ddot{P}_{x,\text{ref}}}{\|\ddot{\mathbf{P}}_{\text{ref}}\|}, \frac{\ddot{P}_{y,\text{ref}}}{\|\ddot{\mathbf{P}}_{\text{ref}}\|}, \frac{\ddot{P}_{z,\text{ref}}}{\|\ddot{\mathbf{P}}_{\text{ref}}\|} \right]^T \tag{17}$$

where $\dot{\mathbf{P}}_{\text{ref}} = d\mathbf{P}_{\text{ref}}/dt$ and $\ddot{\mathbf{P}}_{\text{ref}} = d^2\mathbf{P}_{\text{ref}}/dt^2$. By defining the binormal vector $\mathbf{b}(t) = \mathbf{t}(t) \times \mathbf{n}(t)$, a moving local coordinate frame, namely, a Frenet frame [17], on the tool-path at reference tool center point ($\mathbf{P}_{\text{ref}}(t)$) is defined as ($[\mathbf{t}(t), \mathbf{n}(t), \mathbf{b}(t)]_{3\times 3}$). The Frenet frame in Cartesian coordinates is shown in Fig. 5(a) and modified as

$$\mathbf{F}(t) = \begin{bmatrix} t_x & n_x & b_x & 0 & 0 \\ t_y & n_y & b_y & 0 & 0 \\ t_z & n_z & b_z & 0 & 0 \\ 0 & 0 & 0 & 1 & 0 \\ 0 & 0 & 0 & 0 & 1 \end{bmatrix} \tag{18}$$

to include the rotation errors. The following coordinate transformation holds:

$$\mathbf{e}(t) = \mathbf{F}(t)\mathbf{e}_F(t) \leftrightarrow \mathbf{e}_F(t) = \mathbf{F}^T(t)\mathbf{e}(t) \tag{19}$$

where $\mathbf{F}^T = \mathbf{F}^{-1}$, and $e = [e_x, e_y, e_z, e_a, e_c]^T$ and $\mathbf{e}_F(t) = [e_t, e_n, e_b, e_a, e_c]^T$ are vectors that contain tracking errors of the tool tip in the workpiece coordinate system and in the Frenet frame, respectively. As shown in Fig. 5(a), the vector sums of the errors in normal and binormal directions represent an approximation to the contour error vector as

$$\boldsymbol{\varepsilon} \cong \boldsymbol{e}_n + \boldsymbol{e}_b \tag{20}$$

If the tool-path does not contain sharp curvatures and the feeds were low, the contouring error vector expressed in Eq. (20) is sufficiently accurate. However, at high speed contouring, the limited control bandwidth of the drives creates a time delay between the reference and actual positions of the tool. The tracking errors of the rotary drives may offset the workpiece and can even cause the actual tool position to lead the reference trajectory during five-axis machining. The delay or lead time between the reference and the actual tool tip positions is estimated from the error in tangent direction (e_t) as

$$t_d = \frac{e_t}{\sqrt{\dot{P}_{x,\text{ref}}^2 + \dot{P}_{y,\text{ref}}^2 + \dot{P}_{z,\text{ref}}^2}} \tag{21}$$

and is used to shift the Frenet frame in time as follows:

$$\tilde{\mathbf{F}} = \mathbf{F}(t - t_d) \tag{22}$$

Since the reference trajectory is generated in advance, one can simply use the shifted Frenet frame ($\tilde{\mathbf{F}}$) and utilize the normal and

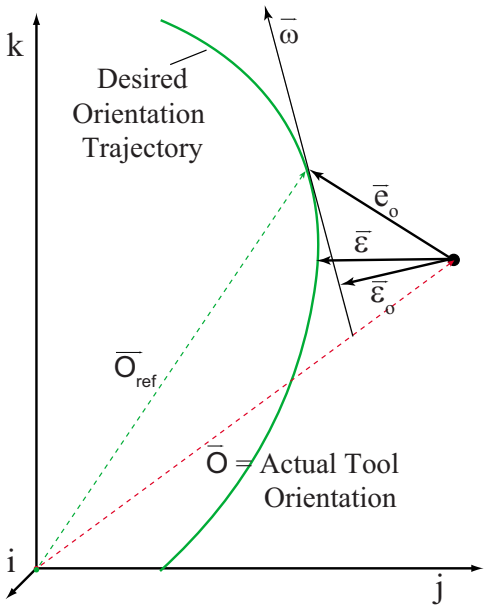

Fig. 6 Orientation contour error estimation

binormal error components to improve the contour error estimation. Although the direction of the contour error vector is estimated more accurately, such a transformation does not evaluate the amplitude ($|\boldsymbol{\varepsilon}|$) accurately, leading to over- or undercuts during actual contouring control. As illustrated in Fig. 5(*b*), the vector between the current and the delayed reference positions is expressed as

$$\mathbf{h} = \begin{bmatrix} \mathbf{P}_{\text{ref}}(t) - \mathbf{P}_{\text{ref}}(t - t_d) \\ 0 \\ 0 \end{bmatrix}, \quad \mathbf{h} \in \Re^{5\times 1} \tag{23}$$

and its representation on $\tilde{\mathbf{F}}$ is computed by

$$\mathbf{h}_F = \tilde{\mathbf{F}}^T \mathbf{h} \tag{24}$$

In order to correct the estimation, only the normal and binormal components are used, and the tangent component is excluded by multiplying with $\mathbf{W}=\text{diag}(0,-1,-1,1,1)$,

$$\tilde{\mathbf{h}}_F = \mathbf{W}\mathbf{h}_F \tag{25}$$

The tracking errors on the compensated Frenet frame $\tilde{\mathbf{F}}$ become

$$\tilde{\mathbf{e}}_F = \tilde{\mathbf{F}}^T \mathbf{e} + \tilde{\mathbf{h}}_F \tag{26}$$

As shown in Fig. 5(*b*), the sum of vector components in the normal and binormal directions ($\tilde{e}_n + \tilde{e}_b$) obtained from Eq. (26) more accurately approximates the actual contour error along arbitrary tool-paths.

3.3 Tool Orientation Contour Error Estimation. As shown in Fig. 6, there is a difference in the definition of tool orientation tracking error vector $\mathbf{e}_o$, and the actual orientation contour error vector $\boldsymbol{\varepsilon}$, both defined in the spherical coordinate system. The orientation tracking error vector is measured from the current tool orientation ($\mathbf{O}$) to the current reference orientation ($\mathbf{O}_{\text{ref}}$). By simply minimizing the tracking errors of the rotary drives, the orientation tracking errors can be eliminated. However, doing so does not necessarily rotate the tool closer to the desired orientation trajectory. The tool orientation may be corrected by eliminating the approximated contour error vector $\boldsymbol{\varepsilon}_0$ (see Fig. 6).

Similar to the Cartesian contour error approximation, the orientation contour error vector is predicted by transforming the tracking errors to obtain the vector that is normal to the reference trajectory as

$$\boldsymbol{\varepsilon}_o = \begin{bmatrix} \varepsilon_{oi} \\ \varepsilon_{oj} \\ \varepsilon_{ok} \end{bmatrix} = \mathbf{e}_o - \frac{\boldsymbol{\omega}}{|\boldsymbol{\omega}|}\frac{\mathbf{e}_o \cdot \boldsymbol{\omega}}{|\boldsymbol{\omega}|} \tag{27}$$

where $\boldsymbol{\omega}=[\omega_i \omega_j \omega_k]^T$ is the angular velocity vector. Normalizing the velocity of the tool axis, $\bar{\boldsymbol{\omega}}=\boldsymbol{\omega}/|\boldsymbol{\omega}|$, we can rewrite Eq. (27) as

$$\boldsymbol{\varepsilon}_o = \mathbf{e}_o - \bar{\boldsymbol{\omega}}(\mathbf{e}_o \cdot \bar{\boldsymbol{\omega}}) \tag{28}$$

From the kinematics of the five-axis machine tool, it is known that the orientation Jacobian ($\mathbf{J}_O$) in Eq. (1) relates the rotary axis velocities ($\mathbf{v}=[v_a, v_c]^T$) to the orientation velocity of the tool

$$\bar{\boldsymbol{\omega}} = k\mathbf{J}_o\bar{\mathbf{v}} \tag{29}$$

where $\bar{\mathbf{v}}=\mathbf{v}/|\mathbf{v}|$ is the unit vector velocity in the *M*-system and $k=|\boldsymbol{\omega}|/|\mathbf{v}|$ is a scalar.

In addition, assuming that the orientation errors are compensated with small drive rotations within the control sampling interval $T=1$ msec(millisecond), we can use the following approximation:

$$\mathbf{e}_o \approx \mathbf{J}_O\mathbf{e}_R \tag{30}$$

where $\mathbf{e}_R=[e_a, e_c]^T$ is the array containing the individual rotary drive errors. Substituting Eqs. (29) and (30) into (28) results in

$$\boldsymbol{\varepsilon}_o = \mathbf{J}_O\mathbf{e}_R - k^2\mathbf{J}_O\bar{\mathbf{v}}\bar{\mathbf{v}}^T\mathbf{J}_O^T\mathbf{J}_O\mathbf{e}_R \tag{31}$$

Using Eq. (29) and properties of the unit vectors ($\bar{\boldsymbol{\omega}}, \bar{\mathbf{v}}$), it can be shown that

$$\bar{\mathbf{v}}^T\bar{\mathbf{v}} = \bar{\boldsymbol{\omega}}^T\bar{\boldsymbol{\omega}} = k^2\bar{\mathbf{v}}^T\mathbf{J}_O^T\mathbf{J}_O\bar{\mathbf{v}} = 1 \rightarrow k^2\bar{\mathbf{v}}^T\mathbf{J}_O^T\mathbf{J}_O = \bar{\mathbf{v}}^T \tag{32}$$

which allows us to simplify Eq. (31) as

$$\boldsymbol{\varepsilon}_o = \mathbf{J}_O\underbrace{[\mathbf{e}_R - \bar{\mathbf{v}}(\bar{\mathbf{v}} \cdot \mathbf{e}_R)]}_{\boldsymbol{\varepsilon}_R} \tag{33}$$

As a result, the relationship between the tool orientation contour error ($\boldsymbol{\varepsilon}_o$) in the *P*-system and the corresponding rotary drive errors ($\boldsymbol{\varepsilon}_R=[\varepsilon_a, \varepsilon_c]$) in the *M*-system is obtained from Eq. (33) as

$$\boldsymbol{\varepsilon}_R = \begin{bmatrix} \varepsilon_a \\ \varepsilon_c \end{bmatrix} = \mathbf{e}_R - \bar{\mathbf{v}}(\bar{\mathbf{v}} \cdot \mathbf{e}_R) \tag{34}$$

4 Implementation and Experimental Results

The proposed contouring error prediction models are experimentally validated on a five-axis machine tool shown in Fig. 7. The in-house developed research CNC has an open architecture, which allows rapid implementation of trajectory generation and control laws. The Cartesian *x*-*y* table carries the rotary drives, and the *z*-axis carries the spindle. The Cartesian drives have 2.9 μm encoder resolutions. The rotary table is driven by the *a* and *c* drives equipped with 8.7 μrad resolution encoders where the offset between their axis or rotation is $a_2=70$ mm. The dynamic parameters of the drives identified experimentally [18] are presented in Table 1.

All five drives are individually controlled by robust sliding mode controllers (SMCs) in order to obtain higher tracking performance. The design procedure is presented by Altintas et al. [19] where the sliding surface is based purely on the tracking errors of the individual axes (Eq. (12)). Thus, the SMC of each axis drive is tuned separately, and the bandwidth of each Cartesian axis is closely matched in order to obtain better contouring performance (see Table 2).

The proposed contour estimation, as well as the robust axis control algorithms, was implemented on the LABVIEW RT© system comprised by two personal computers for real-time computation of the control law, and a field programmable gate array (FPGA)

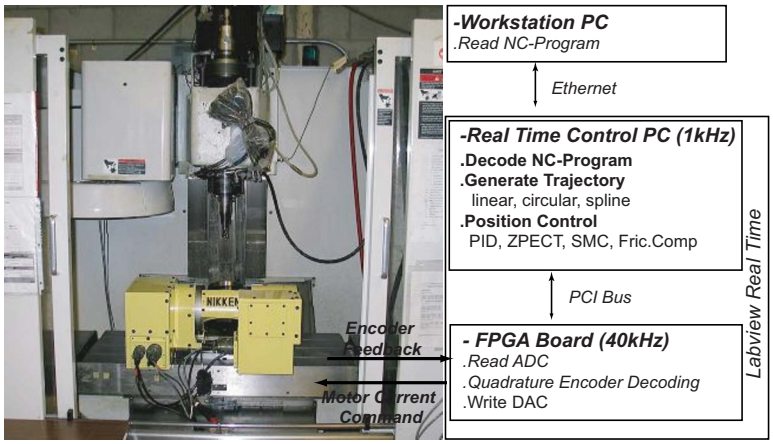

Fig. 7 Five-axis machine tool

card for data acquisition and decoding of the encoder signals. The sampling rate of the control loop is fixed to 1 kHz.

The effectiveness of the proposed five-axis contour error estimation algorithms is demonstrated on a tool-path that contains a circular contour for the tool tip motion and smoothly varying orientation for the tool axis.

The reference five-axis test tool-path is analytically given by

$$\left.\begin{aligned} P_{x\mathrm{ref}} &= 15\cos(l) + 5\sin(l) \\ P_{y\mathrm{ref}} &= 15\sin(l) - 5\cos(l) \\ P_{z\mathrm{ref}} &= 15l \\ a_{\mathrm{ref}} &= -\sin^{-1}(\sin(l)/\sqrt{5}) \\ c_{\mathrm{ref}} &= -\tan(\cos(l)/\sqrt{5}) \end{aligned}\right\} \quad l = 0 \cdots 4\pi \qquad (35)$$

and shown in Fig. 8. The reference path of the tool orientation continuously changes as shown in Fig. 8(*b*). The path of the tool tip follows a circular motion in the *x*-*y* plane, and at the same time the cutter moves in the *z* direction where the total distance of travel along the workpiece is about 273.87 mm. The reference tool-path is interpolated by generating a smooth trajectory with a maximum cruise feed of 50 mm/s and cubic acceleration/decelerations not exceeding 1500 $\mathrm{mm/s^2}$.

In order to investigate the accuracy of the proposed five-axis tool tip contour error computation methods, the basic Frenet frame (Eq. (20)), shifted Frenet frame (Eq. (22)), and the compensated Frenet frame (Eq. (26)) are compared against the true tool tip contour errors as shown in Fig. 9. The true contouring errors are calculated through an iterative search of the shortest distance between the tool tip position and the actual path as presented by Erkorkmaz and Altintas [5], measured in the workpiece coordinate system. The proposed compensated Frenet frame approximation provides the most accurate estimation of the contour errors as shown in Fig. 9(*a*). Severe peaks in the contour error trend can be observed at times ~1 s, 2.2 s, 3.5 s, and 5 s during air cutting. In addition, relatively smaller jumps occur in between at ~1.5 s, 3 s, 3.5 s, and 4.2 s. As the rotational axes go through a direction reversal during five-axis operation, the joint velocity changes rapidly with high acceleration, and, at the same time, the Coulomb friction at the joint acts as a sudden step disturbance to the drive. Each axis controller deals with the disturbance individually and tries to track the high acceleration reference command. The disturbance is rejected in finite time, and severe tracking error at the axis level occurs jeopardizing the coordination between the drives. This deteriorates the contouring performance severely. Thus, contour error peaks in Fig. 9(*a*) coincide with the locations when the *a* rotary axis goes through velocity reversal, and smaller error peaks are related to the tracking performance of the *c* axis (see Figs. 10(*a*) and 10(*b*)). This indicates that during five-axis machining not only the Cartesian but also the rotary drives contribute strongly to the contouring performance. A closer view of the estimation errors of the basic, delayed, and compensated Frenet frame is shown in Fig. 9(*b*). All the proposed methods estimate the contour errors within an acceptable average estimation discrepancy (0.01–0.05 μm). The most severe cases occur when the contour error spikes above 300 μm where the actual tool tip has its maximum lag from the reference point. This lag can be observed from the delay time computed from Eq. (22) and plotted in Fig. 9(*c*). The basic and compensated Frenet frame approximations show good performance even at these locations with estimation errors as high as 0.1 μm and 0.05 μm, respectively.

Table 1 Drive parameters

	x -axis	*y* -axis	*z* -axis	*a* -axis	*c* -axis
$m=J/K_aK_tr_g$	0.00162 V s^2/mm	0.00174 V s^2/mm	0.00296 V s^2/mm	0.00682 V s^2/rad	0.00054 V s^2/rad
$c=B/K_aK_tr_g$	0.00681 V s/mm	0.00863 V s/mm	0.01518 V s/mm	0.01964 V s/rad	0.00368 V s/rad

Table 2 Five-axis SMC parameters (SISO scheme)

SMC parameters	*x* -axis	*y* -axis	*z* -axis	*a* -axis	*c* -axis
ω_n (rad/s)	200	200	180	150	200
K_s (V/nm s) (V/rad s for rotary drives)	7	5	5	0.5	1
Disturbance adaptation gain Γ (V/mm or rad)	25	30	15	3	3

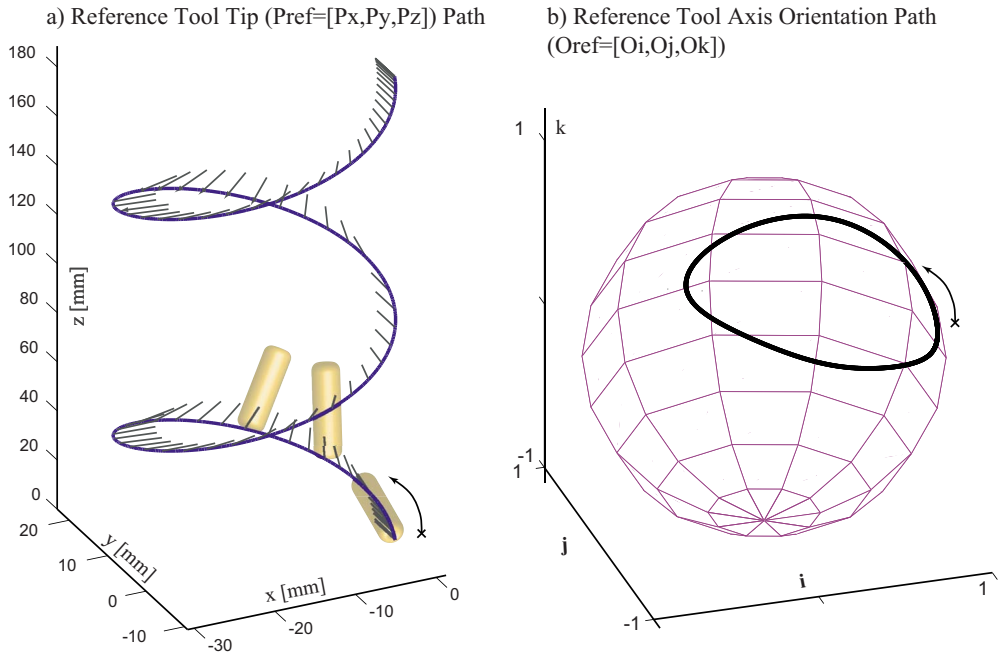

Fig. 8 Experimental tool-path

As a result, both the basic and the compensated Frenet frame methods prove to be sufficiently accurate for contouring control even when the tool tip deviates high from the desired path. On the other hand, the delayed Frenet frame shows the worst performance confirming that the offset **h** in Eq. (23) must be compensated to estimate the amplitude of the contour error accurately.

Similar to the Cartesian case, the actual orientation contour error vector can be obtained by iteratively finding the closest normal point to the actual reference orientation tool-path in spherical coordinates. The actual orientation contour error vector (ε) is computed and transformed into the corresponding a and c rotary drive tracking errors ($\varepsilon_{a,c}$) using the orientation Jacobian (Eq. (30))

$$\varepsilon_{A,C} \approx \mathbf{J}_O \varepsilon \tag{36}$$

and compared against the proposed analytical estimation given in Eq. (34). Figure 10 represents the experimentally recorded rotary drive tracking errors, as well as the true and estimated orientation contour errors expressed in drive coordinates. As shown in Figs. 10(a) and 10(b), the transformation of the orientation contour errors computed from Eqs. (30) and (34) match, and they both show distinct error trends in comparison to the tracking errors of the rotary drives. Rotary drive tracking errors show peaks due to the Coulomb friction at path locations when a and c axes go through velocity reversals. The orientation contour error components mainly follow the tracking errors, indicating that the motion should be synchronized. However, deviations between the trends occur especially when the synchronization is lost as one rotary drive is exposed to a velocity reversal yielding high tracking errors and the other one does not. In Fig. 10(a) one can see that the a rotary drive tracking and orientation error trends differ from each other around 0.5 s, 1.5 s, 3 s, and 4 s on the time scale, corresponding to the locations where the c rotary drive has its highest tracking errors. Similar observation can be made for the c axis at 1 s, 2.5 s, 3.5 s, and 5 s, indicating that elimination of orientation contour errors is crucial in establishing synchronization of the drives toward improving the part accuracy. Figures 10(c) and 10(d) show the deviation of the proposed analytical

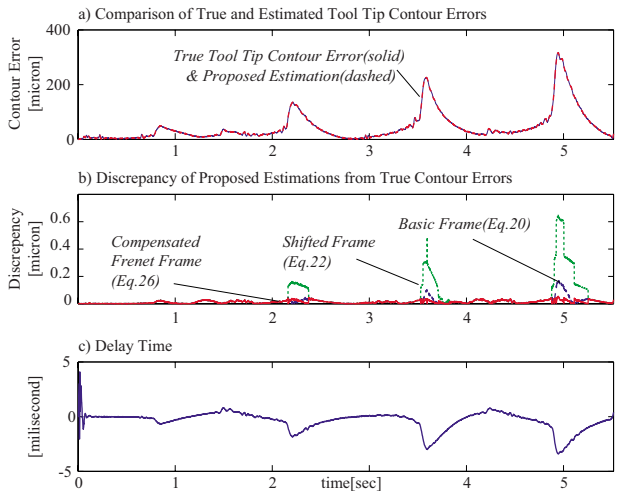

Fig. 9 Comparison of tool tip contouring estimations

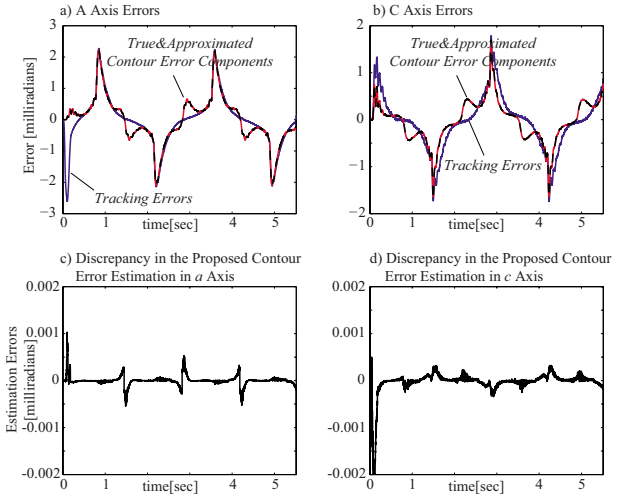

Fig. 10 Orientation contour errors

orientation contour error estimation from the measured values. The maximum deviation is less than 6 μrad for both a and c drives. Considering that the rotary encoders have a resolution of 8.7 μrad, the proposed estimation is valid and suitable for designing orientation contour controller, which is presented in the Part II of this paper.

5 Conclusion

The main concerns during five-axis contouring are the tool tip and the tool orientation contour errors. The kinematic model of five-axis machine tools shows that all five physical drives influence tool tip positioning accuracy while the tool axis orientation errors are caused only by the rotary drives. In this paper, the kinematics and rigid body dynamics of five axes, namely, three translational and two rotary drives, are combined to predict tool tip and tool orientation errors that produce contouring errors on the machined part surface. It is shown that even if the tracking accuracies of all five drives are individually greatly improved by high bandwidth, robust controllers, the overall contouring error of five-axis tool-paths can still be significant due to the path curvature and the kinematics of the machine. Instead of controlling each drive individually, the experimentally validated real-time contouring error estimation model allows the design of a global, sliding mode controller, which simultaneously controls all five drives with the objective of achieving high path tracking accuracy. This controller improves the path tracking accuracy and is presented in Part II of this series.

Acknowledgment

This research is supported by National Sciences and Engineering Research Council of Canada (NSERC) Discovery and Virtual Machining Chair Grants and AUTO21 CM03 Micro Milling Grant.

References

[1] Tsutsumi, M., and Saito, A., 2003, "Identification and Compensation of Systematic Deviations Particular to 5-Axis Machining Centers," Int. J. Mach. Tools Manuf., **43**(8), pp. 771–780.
[2] Koren, Y., 1983, *Computer Control of Manufacturing Systems*, McGraw-Hill, New York.
[3] Koren, Y., and Lo, C.-C., 1980, "Cross-Coupled Biaxial Computer Control for Manufacturing Systems," ASME J. Dyn. Syst., Meas., Control, **102**, pp. 265–272.
[4] Koren, Y., and Lo, C.-C., 1991, "Variable-Gain Cross-Coupling Controller for Contouring," CIRP Ann., **40**(1), pp. 371–374.
[5] Erkorkmaz, K., and Altintas, Y., 1998, "High Speed Contouring Control Algorithm for CNC Machine Tools," *Proceedings of the ASME Dynamic Systems and Control Division*, ASME International Mechanical Engineering Congress and Exposition, DSC 64, pp. 463–469.
[6] Chiu, G. T.-C., and Tomizuka, M., 2001, "Contouring Control of Machine Tool Feed Drive Systems: A Task Coordinate Frame Approach," IEEE Trans. Control Syst. Technol., **9**(1), pp. 130–139.
[7] Yeh, S.-S., and Hsu, P.-L., 2002, "Estimation of the Contouring Error Vector for the Cross-Coupled Control Design, IEEE/ASME Trans. Mechatron., **7**(1), pp. 44–51.
[8] Peng, C.-C., and Chen, C.-L., 2007, "Biaxial contouring Control With Friction Dynamics Using a Contour Index Approach," Int. J. Mach. Tools Manuf., **47**(10), pp. 1542–1555.
[9] Katz, R., Yook, J., and Koren, Y., 2004, "Control of a Non-Orthogonal Reconfigurable Machine Tool," ASME J. Dyn. Syst., Meas., Control, **126**(2), pp. 397–405.
[10] Lin, R.-S., and Hu, C. W., 1999, "Modeling of the Dynamic Contour Error of Five-Axis CNC Machine Tools," ASME Dynamic Systems Control and Control Division, Ver. 67, pp. 861–868.
[11] Lo, C.-C., 2002, "A Tool-Path Control Scheme for Five-Axis Machine Tools," Int. J. Mach. Tools Manuf., **42**(1), pp. 79–88.
[12] Langeron, J.-M., Duc, E., Lartigue, C., and Bourdet, P., 2004, "A New Format for 5-Axis Tool Path Computation, Using Bspline Curves," CAD, **36**(12), pp. 1219–1229.
[13] Tutunea-Fatan, O. R., and Feng, H.-Y., 2004, "Configuration Analysis of Five-Axis Machine Tools Using a Generic Kinematic Model," Int. J. Mach. Tools Manuf., **44**(11), pp. 1235–1243.
[14] Bohez, E. L. J., 2002, "Five-Axis Milling Machine Tool Kinematic Chain Design and Analysis," Int. J. Mach. Tools Manuf., **42**(4), pp. 505–520.
[15] Jung, Y. H., Lee, D. W., Kim, J. S., and Mok, H. S., 2002, "NC Post-Processor for 5-Axis Milling Machine of Table-Rotating/Tilting Type," J. Mater. Process. Technol., **130–131**, pp. 641–646.
[16] Devanit, J., and Hartenberg, R. S., 1955, "A Kinematic Notation for Lower Pair Mechanisms Based on Matrices," ASME J. Appl. Mech., **22**(2), pp. 215–221.
[17] Do Carmo, M. P., 1976, *Differential Geometry of Curves and Surfaces*, Prentice-Hall, Englewood Cliffs, NJ.
[18] Erkorkmaz, K., and Altintas, Y., 2001, "High Speed CNC System Design: Part II—Modeling and Identification of Feed Drives," Int. J. Mach. Tools Manuf., **41**(10), pp. 1487–1509.
[19] Altintas, Y., Erkorkmaz, K., and Zhu, W.-H., 2000, "Sliding Mode Controller Design for High Speed Drives," CIRP Ann., **49**(1), pp. 265–270.